Full-Field Subwavelength Imaging Using a Scattering Superlens

Chunghyun Park,[1,2] Jung-Hoon Park,[1] Christophe Rodriguez,[1,2] HyeonSeung Yu,[1] Minkwan Kim,[2]
Kyoungsuk Jin,[3] Seungyong Han,[4] Jonghwa Shin,[5] Seung Hwan Ko,[4] Ki Tae Nam,[3]
Yong-Hee Lee,[1] Yong-Hoon Cho,[1,2,†] and YongKeun Park[1,*]

[1]*Department of Physics, Korea Advanced Institute of Science and Technology, Daejeon 305-701, Republic of Korea*
[2]*Graduate School of Nanoscience and Technology and KI for the NanoCentury,*
Korea Advanced Institute of Science and Technology, Daejeon 305-701, Republic of Korea
[3]*Department of Material Science and Engineering, Seoul National University, Seoul 151-742, Republic of Korea*
[4]*Department of Mechanical Engineering, Seoul National University, Seoul 151-742, Republic of Korea*
[5]*Department of Materials Science and Engineering, Korea Advanced Institute of Science and Technology, Daejeon 305-701,*
Republic of Korea
(Received 8 July 2014; published 9 September 2014)

Light-matter interaction gives optical microscopes tremendous versatility compared with other imaging methods such as electron microscopes, scanning probe microscopes, or x-ray scattering where there are various limitations on sample preparation and where the methods are inapplicable to bioimaging with live cells. However, this comes at the expense of a limited resolution due to the diffraction limit. Here, we demonstrate a novel method utilizing elastic scattering from disordered nanoparticles to achieve subdiffraction limited imaging. The measured far-field speckle fields can be used to reconstruct the subwavelength details of the target by time reversal, which allows full-field dynamic super-resolution imaging. The fabrication of the scattering superlens is extremely simple and the method has no restrictions on the wavelength of light that is used.

Since the first experimental demonstration of the near-field scanning optical microscope (NSOM) [1], various methods to probe the near fields have been proposed. The field of bioimaging has shown the largest number of new techniques due to the direct need to use visible wavelengths and observation in a nonvacuum environment. Although the currently developed methods are comprised of multiple unique ideas, the common goal of all super-resolution techniques is the effective delivery of the high spatial frequency components of the target object's angular spectrum, which are evanescent and are restricted to distances smaller than the wavelength of light from the object of interest.

Here, we propose to use multiple scattering in turbid media to deliver the near-field wave vectors to the observable far field, which allows optical subdiffraction limited imaging using conventional optics. Similar to the hyperlens [2] or in structured illumination [3] where a specific near-field mode corresponds to a corresponding far-field mode, multiple scattering induces the mixture and transfer between the far and near fields.

Because elastic scattering is described by Maxwell's equations, which has time-reversal symmetry, multiple scattering of light exhibits time-reversal symmetry no matter how complicated and random each scattering event is. This property has allowed fascinating demonstrations such as the removal of inhomogeneity in the generation of photon echoes [4] or perfect absorption which is the

opposite of lasing [5]. In imaging, multiple scattering and the principle of time reversal have been capitalized in reconstructing the incident field prior to multiple scattering [6–8]. In the microwave region, it has also been shown that scattering materials placed in the near field of a target object can scatter the near fields into propagating far-field components [9,10]. More recently, similar phenomena have been shown numerically in the optical region utilizing subwavelength coupled resonators [11] and subwavelength imaging has been demonstrated by using the combination of the memory effect and a high refractive index material [12]. Recently, our group has demonstrated the utilization of multiple scattering for the direct access to the optical near fields to obtain a subwavelength focus via the control of the far fields [13]. Here, we demonstrate that by measuring the near-field transmission matrix (TM) turbid media can be used as a near-field lens, which allows real-time super-resolution imaging in the visible regime.

To reconstruct an image beyond the diffraction limit, the input modes of the TM must include information about the near fields. In our approach, a pointlike source from the tip aperture of a NSOM is used to generate input modes that include high evanescent spatial frequency components. Both near- and far-field components of the focus at the tip aperture are scattered into the turbid medium since the tip is in physical contact. When the TM connecting the point source and the resulting speckle field through the turbid medium is measured holographically, information
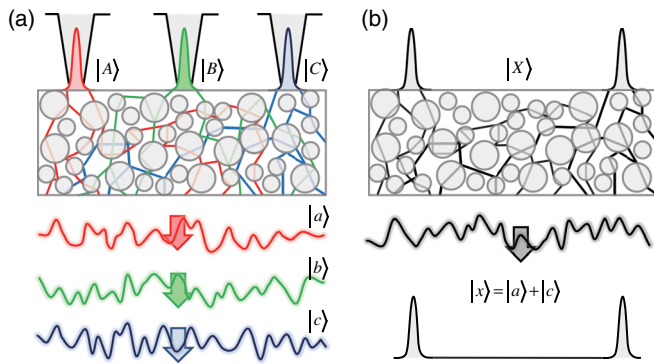
FIG. 1 (color online). Schematic diagram of experimental concept. (a) Measurement of the TM with a pointlike source generated by a near-field aperture as the input basis. The TM is composed of speckle fields propagating through the turbid medium from the near-field aperture. $|a\rangle$, $|b\rangle$, $|c\rangle$ are corresponding speckle fields after the turbid medium as a response to the pointlike illuminating fields $|A\rangle$, $|B\rangle$, $|C\rangle$ on the turbid medium, respectively. (b) Recovery of the original field on the turbid medium from the speckle field generated by an arbitrary sample. The speckle field $|x\rangle$, which is generated by the sample field $|x\rangle$. is multiplied by the time-reversed TM (TM†), which is equivalent to decomposing $|x\rangle$ into a linear combination of $|a\rangle$, $|b\rangle$, $|c\rangle$ with the appropriate complex coefficients.

about the fine structures of the point source is contained in the TM [14].

The idea is schematically illustrated in Fig. 1. Each column of the TM is composed of speckle fields propagating through the turbid medium resulting from the near-field aperture at each scanning position. For example, the

output modes $|a\rangle$, $|b\rangle$, $|c\rangle$ are the speckle fields that have propagated through the turbid medium as a response to the pointlike illuminating fields (the input modes $|A\rangle$, $|B\rangle$, $|C\rangle$ on the turbid medium, respectively). The measured speckle fields $|a\rangle$, $|b\rangle$, $|c\rangle$ then constitute the 1st, 2nd, and 3rd columns of the TM. In other words, the TM is defined by using the pointlike spatial modes as the input basis and the corresponding output two-dimensional (2D) speckle field measured is converted into each column vector. The number of rows determines the accuracy of image recovery and the maximum field of view achievable, because the number of rows (262 144) in our currently measured TM oversamples the degrees of freedom compared to the number of columns (4096 or 8192).

For image recovery using the measured TM, the principle of time reversal is used [15–18]. As shown in Fig. 1(b), the measured speckle field of an arbitrary sample that is placed on the turbid medium can be sent back through the turbid medium to result in the same shape as the original sample (neglecting the lost unrecorded scattered light) if an appropriate phase conjugate mirror can be made. For solely imaging purposes, we can reproduce the phase conjugate mirror by using the time reversed TM, which is the conjugate transpose in optics (TM†), and computationally multiply it with the column vector comprising of the measured speckle field, which results in the computation of TM$^\dagger \times$ TM, the time-reversal matrix [6].

The experimental setup used to realize this idea is shown in Fig. 2(a). A Mach-Zehnder interferometer combined with a commercial NSOM system is used to measure the speckle field behind the turbid medium when illuminated
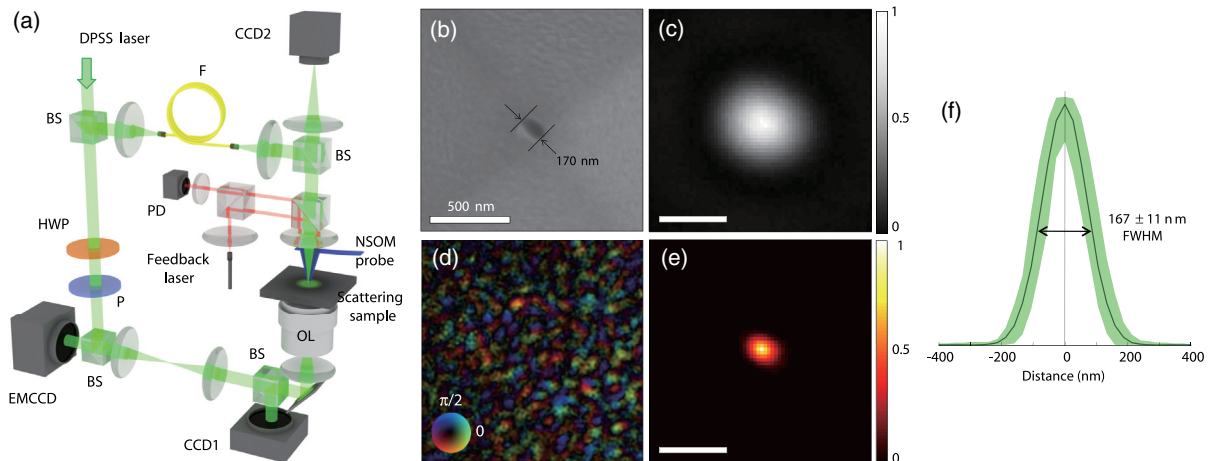

FIG. 2 (color online). Experimental setup and reconstructed point source. (a) A Mach-Zehnder interferometer is incorporated with a commercial NSOM system. BS: beam splitter, P: polarizer, F: optical fiber, HWP: half-wave plate, PD: quadrant photodiode, OL: objective lens. (b) SEM image of the NSOM tip aperture. (c) Far-field image of light radiating from the tip obtained with an objective lens of 0.8 NA. The diffraction-limited beam spot is about 420 nm. (d) Measured amplitude and phase of the far-field speckle pattern after light from the NSOM aperture has scattered through the turbid medium and has propagated through over 1 m of far-field optics. The color represents the phase while brightness represents the normalized amplitude. (e) Reconstructed image of the same light source using the TM and the principle of time reversal. (f) FWHM of the reconstructed beam spot is about 167 nm. Thick black line represents the average of 150 experimental sets (thick green stripe represents maximum and minimum of the experimental data, respectively).

by a near-field aperture. Light from a 532-nm laser is split into the sample and reference beams where the sample beam is focused onto the rear plane of the near-field tip aperture. The focused beam then propagates through the turbid medium and the resulting speckle field is combined with the reference beam and measured using the electron-multiplying charge-coupled device (EMCCD) after being magnified by a 4-f telescopic system. The complex speckle field is then extracted from the measured hologram using standard algorithms in off-axis holography [19,20].

The input modes of the TM are defined by the size of the NSOM aperture [Fig. 2(b)]. Because direct movement of the NSOM tip is not possible in our commercial NSOM system, effective tip movement is realized by shifting the turbid medium and digitally shifting the recorded speckle image accordingly. A scan step of 26.7 nm is chosen to match the EMCCD pixel size of 16 μm through ×600 magnification. In the current setup, measurement of the TM covering an area of 1.71×1.71 μm field of view in steps of 26.7 nm takes 610 seconds in scanning 64×64 points. To demonstrate the proof of principle of the method, the beam from the NSOM tip aperture is chosen as the sample to be reconstructed using the TM. The reconstructed image is shown in Fig. 2(e) where the full width at half maximum (FWHM) of the reconstructed image is 167 ± 11 nm. A far-field image of the beam from the same tip aperture obtained with an objective lens with a numerical aperture (NA) of 0.8 is shown for comparison in Fig. 2(c). A NA of 0.8 was chosen since the far-field speckle field was measured using an objective with NA = 0.8. The diffraction-limited FWHM measured without using the near-field TM is 419 nm in the far-field image and is more than 2.5 times bigger than that of the reconstructed image using the TM. The subwavelength resolution is possible due to the utilization of the near-field TM in contrast to previous reports using diffraction-limited TMs [7,12,21–24]. The spatial resolution of the present technique will be determined by parameters including the near-field speckle correlation, the size of tip aperture, and the effective refractive index. Our previous result, which has a time-reversal relation to the present work, showed that the minimum focus size of 167 nm was mainly determined by the tip aperture size, regardless of the effective refractive index and the near-field speckle correlation [13]. In addition, we should emphasize that the subwavelength imaging capability of our technique results from the conversion of information contained in the near fields to far fields via multiple scattering, not by the effective high refractive index of the scattering medium. We believe that it is possible to enhance the resolution even further if a smaller tip is used for the TM measurement and the turbid medium with even smaller sizes is adopted [20].

To demonstrate subdiffraction limited 2D image transfer, we first emulated a target object by scanning the NSOM probe in an arbitrary shape. The emulated object field is composed of point fields among which one point field exists solely at one time while a real object field is composed of point fields that exist simultaneously at the same time. To eliminate the difference between the emulated field and the real field that would be measured from a real sample, the temporal sum of the fields is used instead of spatial summation. By temporal, we mean that the CCD exposure is kept on during the entire tip scan duration. The emulated speckle field is then finally extracted from an intensity measurement accumulated during the exposure using off-axis holography. After the TM is measured for the particular turbid medium (the scattering superlens), the NSOM probe is scanned in the shape of the target object (the word *NANO* or a triangle). To emulate single-shot imaging, the exposure of the EMCCD is kept on during the scanning of the target shape within the persistence time of our system [20]. By accumulating the speckle fields for each position during scanning, the situation is identical to acquiring a single-shot image of a patterned mask with the particular shape. The traces of the tip movement relative to the turbid medium are depicted in Figs. 3(a) and 3(d), which are convolutions of the tip movement positions and shape of the tip aperture as measured by a scanning electron microscope (SEM). The word *NANO* is written in a rectangular area of 3.1×1 μm^2. The reconstructed image is shown in Fig. 3(c) where a TM constructed by speckle fields obtained from 128×64 pointlike input modes evenly distributed in a 3.41×1.71 μm^2 field of view was used for the reconstruction (the TM size is $8192 \times 262\,144$). The second targeted shape is an isosceles triangle, which has a bottom width of 1 μm. The reconstructed triangle image is shown in Fig. 3(f) where a TM constructed by speckle fields obtained from 64×64 pointlike input modes evenly distributed in a 1.71×1.71 μm^2 square was used for the reconstruction (the TM size is $4096 \times 262\,144$). It can clearly be seen that the near-field TM can effectively deliver subwavelength images to the far field. Furthermore, we demonstrate dynamic full-field imaging by tracking the movement of the NSOM tip [Fig. 3(g)]. In this case, each speckle field is measured at arbitrary time lapses to reconstruct the movement of the subwavelength point source moving along the triangular path. There is no need for ensemble averaging and each single speckle pattern measured at the speed of 10 Hz reconstructs a corresponding wide-field image (see the movie in the Supplemental Material [20]).

The current experimental system has some conditions that must be taken into account for measuring real 2D samples. To transfer the near-field components of a real sample, the contact between the sample and the turbid medium should be within subwavelength distances. For this purpose, the turbid medium was fabricated to have a surface roughness equal to a standard coverslip [20]. Because of practical difficulties in the exact alignment of a macroscopic target (with nanoscopic features) to a
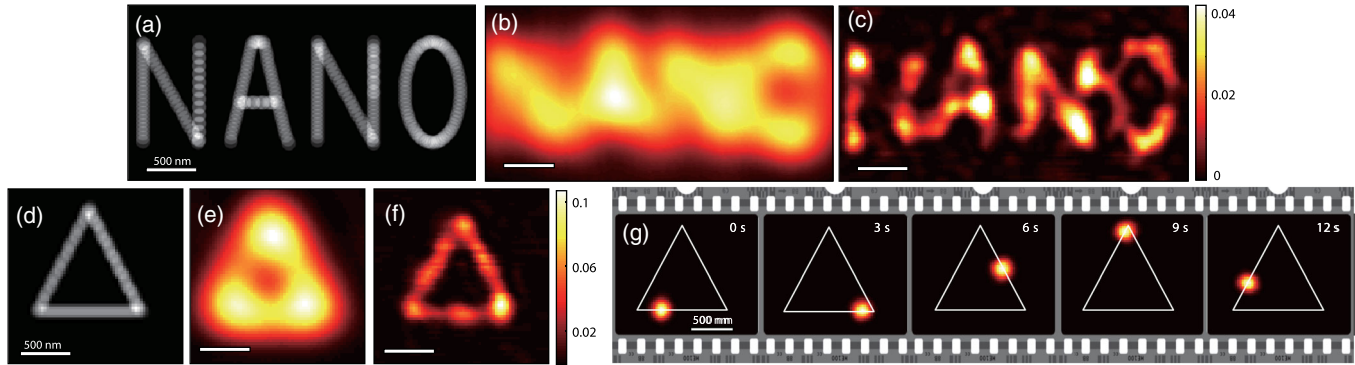
FIG. 3 (color online). Dynamic 2D image reconstruction. (a) Actual loci of the movement of the tip aperture relative to the turbid medium to generate a pseudosample displaying the letters *NANO*. (b) Diffraction-limited image of *NANO*, constructed by convolution of the tip movement with the system's point spread function shown in Fig. 2(c). (c) Reconstructed image using the near-field TM. (d)–(f) Same as in (a)–(c) for a different pattern displaying a triangle. (g) Dynamic full-field imaging where the speckle field is measured dynamically rather than accumulating for the entire pattern generating process. Each full-field image is obtained with a single measurement with a time resolution decided solely by the sensitivity of the EMCCD. Each image shows a higher signal to noise ratio compared with (c),(f) due to effective management of the dynamic range.

microscopic region of the turbid medium, we made a nanoscopic sample directly on a NSOM tip. For this purpose, the tip of a NSOM cantilever was cut and truncated to obtain a rectangle with sides of 630×570 nm. The measured TM for this experiment covered an area of $5.12 \times 5.12 \ \mu m^2$ consisting of 64×64 input modes. The scan step size of the input modes in this case was increased to 80.1 nm, which still satisfies the Nyquist-Shannon sampling theorem with respect to the current system resolution of 167 nm. Because the input field of view increases 9 times compared to the TM used for the reconstruction of the triangle, the reconstructed image has a lower SNR due to the lower degree of freedom ratio γ of 1.13 [20]. The retrieved image clearly agrees with the SEM image and even succeeds in resolving the blockage of light in the obstructed corner (Fig. 4). The concentration of intensity at the other corners is presumably due to the guiding of light along the pyramid interface boundaries.

A key advantage of this technique is that it is scan free and a large field of view can be obtained in a single shot. Although near-field scanning of the input modes is needed for the measurement of the TM, the actual imaging process using the calibrated turbid medium is a single-shot wide-field measurement. This is significantly advantageous compared to other preexisting super-resolution techniques [25–27], which mostly require scanning or image processing from multiple images. The current limiting factor in enhancing the quality or the spatial capacity of the TM lies on the size of the NSOM tip aperture and in the incomplete time-reversal process. For an ideal perfect time reversal, all of the scattered waves should be collected. If the back-scattered speckles are also measured in addition to using a finer NSOM tip to define the input modes, we anticipate that this method can be readily extended to finer resolutions and higher signal to noise ratios. Furthermore, although our system's current signal to noise ratio was sufficient in

obtaining all of the targeted 2D objects, larger and more complex shaped objects can also be more clearly reconstructed if the Tikhonov regularization method is adapted to our reconstruction algorithm. In this case the system noise, which is amplified during time reversal, can be suppressed, resulting in a much more robust reconstruction [7]. Based on the large degree of freedom due to multiple scattering, the wavelength [28] or polarization [29,30] dependent near-field TM can also in principle be measured to allow spectral and polarization sensitive near-field imaging. Furthermore, measuring TMs at multiple temporal frequencies, for instance using a supercontinuum or a wavelength tunable laser for illumination, would also greatly enhance the number of total degrees of freedom available for image reconstruction [31].
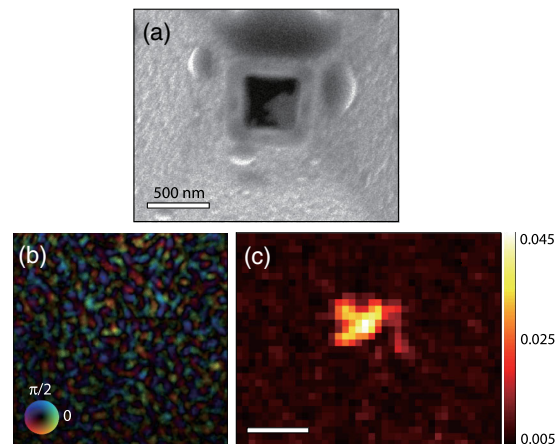

FIG. 4 (color online). Real image reconstruction. (a) SEM image of the rectangular aperture object fabricated by truncating a NSOM probe, (b) measured propagating speckle field with light illuminating the object, and (c) reconstructed image using the near-field TM.

---

[*]yk.park@kaist.ac.kr
[†]yhc@kaist.ac.kr

[1] D. Pohl, W. Denk, and M. Lanz, Appl. Phys. Lett. **44**, 651 (1984).
[2] J. Pendry, Opt. Express **11**, 755 (2003).
[3] M. G. L. Gustafsson, Proc. Natl. Acad. Sci. U.S.A. **102**, 13081 (2005).
[4] N. Kurnit, I. Abella, and S. Hartmann, Phys. Rev. Lett. **13**, 567 (1964).
[5] W. Wan, Y. Chong, L. Ge, H. Noh, A. D. Stone, and H. Cao, Science **331**, 889 (2011).
[6] S. M. Popoff, G. Lerosey, R. Carminati, M. Fink, A. C. Boccara, and S. Gigan, Phys. Rev. Lett. **104**, 100601 (2010).
[7] S. Popoff, G. Lerosey, M. Fink, A. C. Boccara, and S. Gigan, Nat. Commun. **1**, 81 (2010).
[8] T. R. Hillman, T. YamauchiW. Choi, R. R. Dasari, M. S. Feld, Y. Park, and Z. Yaqoob, Sci. Rep. **3**, 1909 (2013).
[9] G. Lerosey, J. de Rosny, A. Tourin, and M. Fink, Science **315**, 1120 (2007).
[10] F. Lemoult, G. Lerosey, J. de Rosny, and M. Fink, Phys. Rev. Lett. **104**, 203901 (2010).
[11] F. Lemoult, M. Fink, and G. Lerosey, Nat. Commun. **3**, 889 (2012).
[12] E. G. Van Putten D. Akbulut J. Bertolotti, W. L. Vos, A. Lagendijk, and A. P. Mosk, Phys. Rev. Lett. **106**, 193905 (2011).
[13] J.-H. Park, C. Park, H. Yu, J. Park, S. Han, J. Shin, S. Hwan Ko, K. Tae Nam, Y.-H. Cho, and Y. Park, Nat. Photonics **7**, 454 (2013).
[14] A. Derode, A. Tourin, and M. Fink, Phys. Rev. E **64**, 036606 (2001).
[15] G. Lerosey, J. de Rosny, A. Tourin, A. Derode, G. Montaldo, and M. Fink, Phys. Rev. Lett. **92**, 193904 (2004).
[16] M. Fink, Sci. Am. **281**, 91 (1999).
[17] Z. Yaqoob, D. Psaltis, M. Feld, and C. Yang, Nat. Photonics **2**, 110 (2008).
[18] M. Tanter, J.-L. Thomas, and M. Fink, J. Acoust. Soc. Am. **108**, 223 (2000).
[19] M. Takeda, H. Ina, and S. Kobayashi, J. Opt. Soc. Am. **72**, 156 (1982).
[20] See Supplemental Material http://link.aps.org/supplemental/10.1103/PhysRevLett.113.113901, which includes Refs. [7,13,14,19], for information on experimental setup, transmission matrix measurement and image reconstruction methods, and additional data.
[21] S. M. Popoff, A. Aubry, G. Lerosey, M. Fink, A. C. Boccara, and S. Gigan, Phys. Rev. Lett. **107**, 263901 (2011).
[22] Y. Choi, T. D. Yang, C. Fang-Yen, P. Kang, K. J. Lee, R. R. Dasari, M. S. Feld, and W. Choi, Phys. Rev. Lett. **107**, 023902 (2011).
[23] Y. Choi, C. Yoon, M. Kim, T. D. Yang, C. Fang-Yen, R. R. Dasari, K. J. Lee, and W. Choi, Phys. Rev. Lett. **109**, 203901 (2012).
[24] I. Vellekoop, A. Lagendijk, and A. Mosk, Nat. Photonics **4**, 320 (2010).
[25] M. J. Rust, M. Bates, and X. Zhuang, Nat. Methods **3**, 793 (2006).
[26] E. Betzig, J. Trautman, T. Harris, J. Weiner, and R. Kostelak, Science **251**, 1468 (1991).
[27] E. H. Rego, L. Shao, J. J. Macklin, L. Winoto, G. A. Johansson, N. Kamps-Hughes, M. W. Davidson, and M. G. Gustafsson, Proc. Natl. Acad. Sci. U.S.A. **109**, E135 (2012).
[28] J. H. Park, C. H. Park, H. Yu, Y. H. Cho, and Y. K. Park, Opt. Lett. **37**, 3261 (2012).
[29] J.-H. Park, C. Park, H. Yu, Y.-H. Cho, and Y. Park, Opt. Express **20**, 17010 (2012).
[30] H. Yu, T. R. Hillman, W. Choi, J. O. Lee, M. S. Feld, R. R. Dasari, and Y. K. Park, Phys. Rev. Lett. **111**, 153902 (2013).
[31] F. Lemoult, G. Lerosey, J. de Rosny, and M. Fink, Phys. Rev. Lett. **103**, 173902 (2009).